Applied Catalysis B: Environmental 197 (2016) 337–342

Contents lists available at ScienceDirect

Applied Catalysis B: Environmental

journal homepage: www.elsevier.com/locate/apcatb

Scanning tunneling microscopy studies of Mn-doped $CeO_x(111)$ interfaces

Elfrida Ginting, Erik Wayne Peterson, Jing Zhou *

Department of Chemistry, University of Wyoming, Laramie, WY 82071, United States

ARTICLE INFO

Article history:
Received 19 December 2015
Received in revised form 19 March 2016
Accepted 11 April 2016
Available online 13 April 2016

Keywords:
Ceria
Manganese
Dopant
Scanning tunneling microscopy
X-ray photoelectron spectroscopy

ABSTRACT

The growth and structure of Mn on reducible ceria were investigated under ultrahigh vacuum conditions with X-ray photoelectron spectroscopy, low energy electron diffraction and scanning tunneling microscopy techniques. Submonolayer coverage of Mn was deposited on well-ordered $CeO_x(111)$ ($1.5 < x < 2$) thin films by physical vapor deposition method at room temperature. Mn is oxidized and formally in the +2 oxidation state on both fully oxidized and partially reduced ceria. Oxidation of Mn is accompanied with the reduction of ceria. STM results show the presence of atomic-layer high islands of Mn forming Mn-O-Ce linkages uniformly distributed on the ceria surface. With heating to higher temperatures, these MnO features can coalesce to form slightly larger two-dimensional structures. Our combined spectroscopy and microscopy studies demonstrate a strong interaction between Mn and ceria supports. Introduction of Mn can form mixed Mn-Ce oxides at the interface which can represent model metal-doped ceria surfaces for further examination of the chemical behavior.

1. Introduction

Ceria exhibits facile reversible transformation from the Ce^{4+} state to the Ce^{3+} state and the formation/annihilation of oxygen vacancies on the surface. Due to unique redox properties and oxygen storage capacity of ceria, supported metal nanoparticles including Ni, Au and Pt can exhibit promising reactivity in catalytic processes including steam reforming of hydrocarbons, water-gas shift and CO oxidation reactions [1–7]. However, ceria can sinter at higher temperatures and is subject to the loss of crucial oxygen storage capacity and redox properties [8,9]. Doping ceria with appropriate metal dopants (i.e., Ti and Zr) can form mixed metal dopant-Ce-O interfaces or mixed solid ceria-based oxides. The additional metal dopant can affect not only the morphology but also its chemical state. Ceria-based mixed oxides can result in increased thermal stability [10,11]. The interaction of metal dopant with ceria can also lower the activation energy needed for the release of oxygen and result in the improvement of redox properties and oxygen storage capacities of ceria. Doped ceria as catalytic supports could better stabilize active metal particles and promote their reactivity [12–18].

To examine the intriguing properties and chemistry at metal dopant-ceria interfaces, it is of crucial importance to determine their surface structures at the atomic/nano scale. For this reason, detailed surface chemistry studies of interactions between metal dopants including Zr, Sn, Ga, W, Mg, Ti, V and Co with ceria have been reported [19–27]. Our group is interested in the study of Mn-doped ceria. Mn can be an appropriate modifier of structural and chemical properties of ceria based on its ionic radius and electronegativity properties. Previous studies have shown that addition of Mn can form Ce-Mn-O solids and significantly increase the stability, oxygen storage capacities and redox properties of ceria [28–30]. Furthermore, manganese oxide is a commonly used material in catalysis. In our previous study, we focused on the detailed X-ray photoelectron spectroscopy (XPS) characterization of the Mn-ceria interaction [31]. As a follow up study, we report in this paper our recent results on the morphology and structure of Mn-doped ceria interfaces formed at room temperature as well as after heating to elevated temperatures to examine their chemical and structural stability by scanning tunneling microscopy (STM). Mn was deposited on well-ordered $CeO_x(111)$ ($1.5 < x < 2$) surfaces at 300 K by physical vapor deposition under ultrahigh vacuum conditions. Considering Mn as a dopant metal to ceria, only submonolayer coverage of Mn was used in our study.

* Corresponding author.
E-mail address: jzhou2@uwyo.edu (J. Zhou).

http://dx.doi.org/10.1016/j.apcatb.2016.04.020
0926-3373/

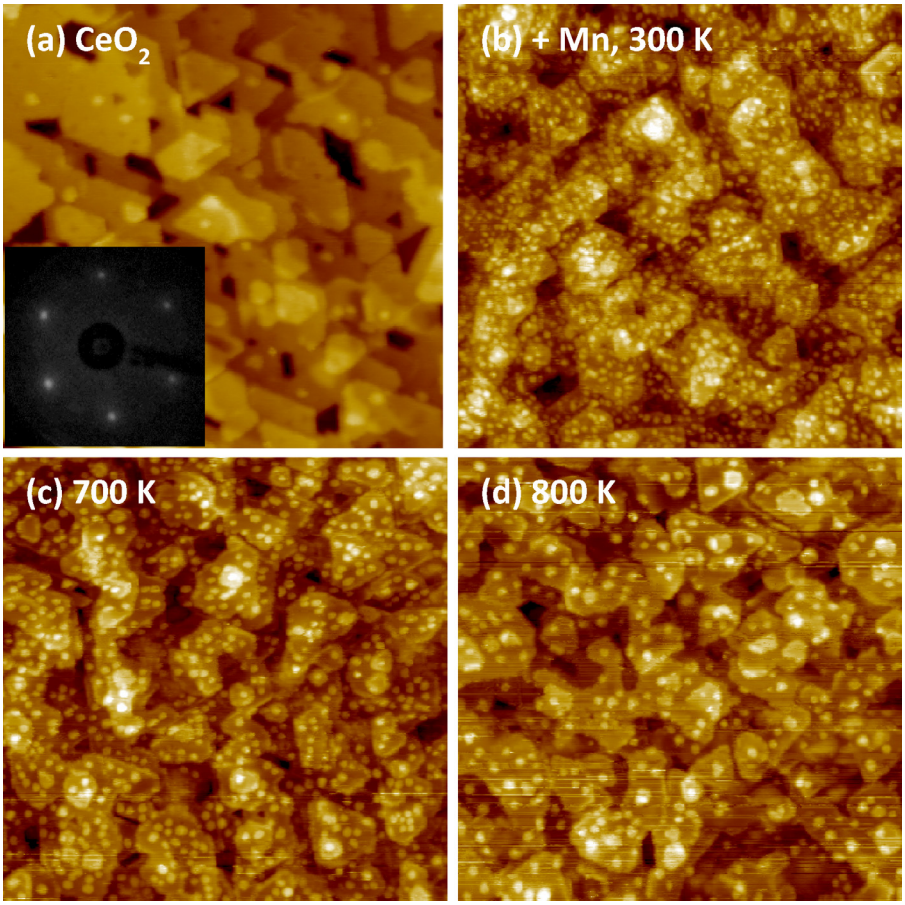

Fig. 1. STM images of a CeO_2(111) thin film surface (a) and with 0.2 ML Mn deposited at 300 K (b) as well as after heating to 700 K (c) and 800 K (d). Image sizes are $120 \times 120\,nm^2$. LEED pattern of the CeO_2(111) surface was shown as an inset in (a).

2. Experimental

All experiments were carried out using a surface analysis apparatus manufactured by Omicron Nanotechnology. The base pressure of the system is below 5×10^{-11} Torr. The instrument is equipped for the growth and characterization of metal nanoparticles and oxide thin films with a variable-temperature scanning tunneling microscope (VT STM XA650), an EA 125 U1 hemispherical electron spectrometer and a DAR 400 twin-anode X-ray source for XPS studies, 4-grid SPECTALEED optics, an ISE 5 cold cathode sputtering ion source, a sample manipulator with e-beam heating capabilities and metal evaporation sources.

A Ru(0001) single crystal (Princeton Scientific Corp., diameter 10 mm, roughness <0.03 μm, orientation accuracy <0.1°) was used as a substrate for the growth of ceria thin films. The crystal was cleaned by Ar ion bombardment with a sample current of ~3 μA followed by annealing at 1300 K for 45 s. Low energy electron diffraction (LEED), STM and XPS were used to confirm the surface order and cleanliness of Ru(0001) prior to the growth of ceria thin films. Fully oxidized CeO_2(111) thin films can be obtained by deposition of Ce on Ru in 2×10^{-7} Torr O_2 at 700 K followed by subsequent heating [32–35]. The Ce flux used for the study is ~0.2 ML/min. Reduced CeO_x(111) thin films can be grown by decreasing the oxygen pressure during Ce deposition. Ce 3d and O 1s XPS spectra were monitored after each film growth to determine the stoichiometric value x in CeO_x. LEED was used to confirm the formation of ceria thin films with the (111) orientation. STM line profile measurement suggests that the films consist of 4–5 Ce-O-Ce layers. Detailed surface structures of the CeO_x(111) surfaces were resolved by previous STM studies [35].

Mn (Goodfellow, purity 99.98+%) was vapor-deposited on to ceria films at 300 K using a home-made E-beam evaporator. In our study, Mn deposition flux of 0.04 ML/min was used, which was obtained by the STM and XPS studies of Mn growth on the bare Ru substrate with a ten-minute deposition at a fixed evaporation power. Mn follows the layer-by-layer growth mode on Ru (0001). Surface coverage of Mn in the unit of monolayer on Ru was determined using the SPIP SPM data analysis software to calculate the flux value. Additionally, the attenuation of the Ru 3d XPS intensity was monitored after Mn deposition and used to estimate the Mn film thickness and corresponding deposition flux. The XPS intensity of Ru 3d decays with the thickness of the Mn film (d) as $I = I_0 \exp(-\frac{d}{\lambda \cos\theta})$. I and I_0 are the integrated peak areas of Ru 3d with and without Mn. Considering the values of 67° for θ according to our XPS setup and 13.4 Å for λ obtained from NIST Electron Effective-Attenuation-Length Database, a flux of ~0.1 Å/min was obtained which can be converted to be ~0.04 ML/min factoring the atomic radius of 140 pm for Mn [36]. Calculated deposition flux value from the XPS study matches well with that from the STM calibration.

STM, XPS and LEED characterizations were performed at room temperature. STM experiments were conducted with an etched W tip. The images were collected with a constant current mode (sample bias: 1.0–3.0 V; tunnelling current: 0.05–0.1 nA). XPS spectra were taken using a Mg Kα radiation (15 KV, 20 mA) with a fixed electron passing energy of 50 eV. An entrance slit size of $6 \times 12\,mm^2$ was used to maximize the XPS signal while ensuring examining

the sample surface exclusively. A typical XPS spectrum was collected with a 0.020 eV step and 0.200 s dwell time and averaged over two scans. Our XPS spectrometer was calibrated by setting the $4f_{7/2}$ binding energy of a bulk gold foil (Alfa Aesar, 0.1 mm thick, 99.9975+%) at 84.0 eV. LEED patterns were taken with a beam energy of 80 eV.

3. Results and discussion

$CeO_2(111)$ exhibits a $p(1.4 \times 1.4)$ LEED pattern as shown in Fig. 1a. The indexing employed for the observed spots is based on the comparison with those from the Ru(0001). Our LEED study indicates that $CeO_2(111)$ film is well-ordered with the (111) plane orientation. It consists of atomically flat terraces separated by steps of ~0.3 nm high with measured distance between two adjacent Ce atoms of ~0.4 nm [35]. Deposition of 0.2 ML Mn on CeO_2 at 300 K maintains the ceria lattice as the $p(1.4 \times 1.4)$ spots of the $CeO_2(111)$ structure were still observed in the LEED pattern. STM image shows the formation of very small bright protrusions (Fig. 1b). They are 1.84 nm wide and 0.18 nm high measured with respect to the ceria terrace. Based on the height measurement, the clusters consist of one atomic-layer of Mn on the $CeO_2(111)$ surface. They are uniform in size with standard deviation values of 0.33 and 0.05 nm for diameter and height, respectively. Furthermore, they exhibit a uniform distribution on the ceria surface with a density of 5.0×10^{12} cm^{-2}. Contrary to metals which have a weaker interaction with CeO_2, preferential adsorption of Mn at the under-coordinated step edges was not observed [37,38]. Our STM data suggests a strong interaction between Mn and ceria, which can result in a short diffusion length of Mn and contribute to the observed growth of small two-dimensional particles. The stability of the particles was examined by annealing at indicated high temperatures for 4 min (Fig. 1c and d). There is a slight increase in the particle diameter to 2.20 nm with a corresponding decrease of the particle density to 4.2×10^{12} cm^{-2} upon heating to 700 K. Further particle coalesce was observed at 800 K with the decreased cluster density of 2.1×10^{12} cm^{-2}. Average particle diameter and height increase to 2.60 and 0.24 nm.

XPS was used to investigate the interaction between Mn and ceria. Mn 2p core level XPS spectrum is broad and complex contributed to the multiple splitting [39–43]. Determination of the Mn valence state can be complicated. Mn has multi-chemical states. Furthermore, the variation of XPS binding energies of Mn 2p from Mn^{2+} to Mn^{4+} is less than 1 eV. Fig. 2a shows the Mn 2p XPS spectrum collected upon 0.2 ML Mn deposition on CeO_2 at 300 K. The observed binding energy positions of 2p doublet peaks centered at ~641.2 and 652.8 eV with a satellite peak about 6 eV higher binding energy are in the range of the literature values for MnO [39,40]. Extensive peak fitting of Mn 2p XPS spectrum as previously reported in detail confirms the presence of Mn^{2+} species in the ceria film [31]. Oxidation of Mn to Mn^{2+} is consistent with the observed partial reduction of ceria as shown in Fig. 2b and c. Ce 3d XPS region contains characteristic peaks originated from different Ce oxidation states (Ce^{3+} and Ce^{4+}) and their 4f configurations, which can be used to examine the oxidation state of cerium in the film [44]. Fully oxidized CeO_2 film shows six peaks which correspond to three pairs of spin-orbit split doublets labeled as U, U″, U‴, V, V″, and V‴. U and V refer to the $3d_{3/2}$ and $3d_{5/2}$ component, respectively. Upon Mn deposition at 300 K, the peaks associated with Ce^{3+} cations (U′, U_0, V′, and V_0) appear in the 3d XPS spectrum which indicates the ceria film gets reduced. Peak decomposition of Ce 3d spectrum as described extensively in our previous paper shows that ~20% of Ce^{4+} ions in the as-grown CeO_2 film are converted to Ce^{3+} cations, resulting in the ceria film with a stoichiometry of $CeO_{1.90}$ [35]. Reduction of Ce upon Mn deposition is consistent with O 1s XPS data. O 1s XPS spectrum of CeO_2 contains a single peak at the binding energy of 529.3 eV which is characteristic of lattice O in ceria [44,45]. A shoulder peak at 531. 9 eV appears with the addition of Mn on the surface. The peak position agrees well with that of defective oxides or surface oxygen ions with low coordination reported in the literature, which confirms the formation of reduced ceria as well as Mn-O-Ce structures in our study [20,21,46,47]. Considering the fact that Mn is in the +2 state, the observed bright protrusions in the STM image can be attributed to MnO clusters.

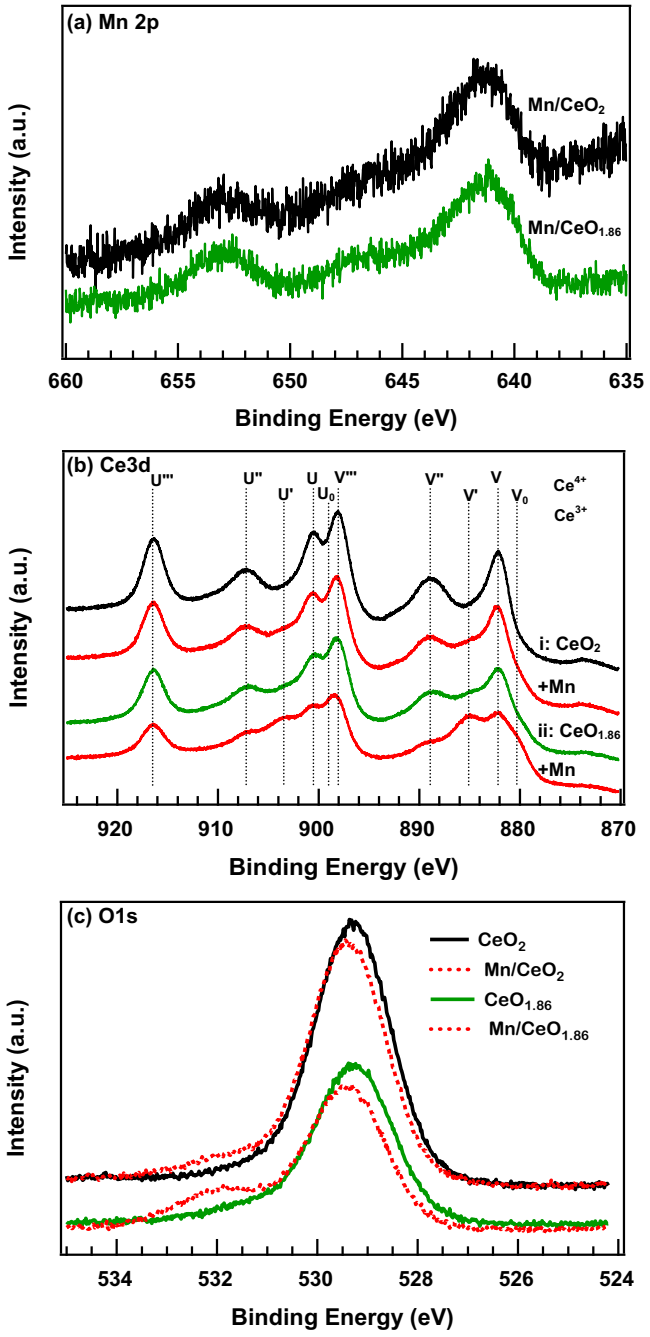

Fig. 2. (a) Mn 2p XPS spectra collected upon 0.2 ML Mn deposition at 300 K on CeO_2 (i) and $CeO_{1.86}$ (ii); (b) and (c) Ce 3d and O 1s XPS data collected from as-grown CeO_2 and $CeO_{1.86}$ as well as upon Mn deposition.

The growth of Mn was investigated on a partially reduced ceria. Shown in Fig. 3a is the STM image of a $CeO_{1.86}$ (111) surface as an example. The film is atomically flat and well-ordered with a comparable $p(1.4 \times 1.4)$ LEED pattern to that of CeO_2. However, surface defects associated with O vacancies and Ce^{3+} cations are suggested

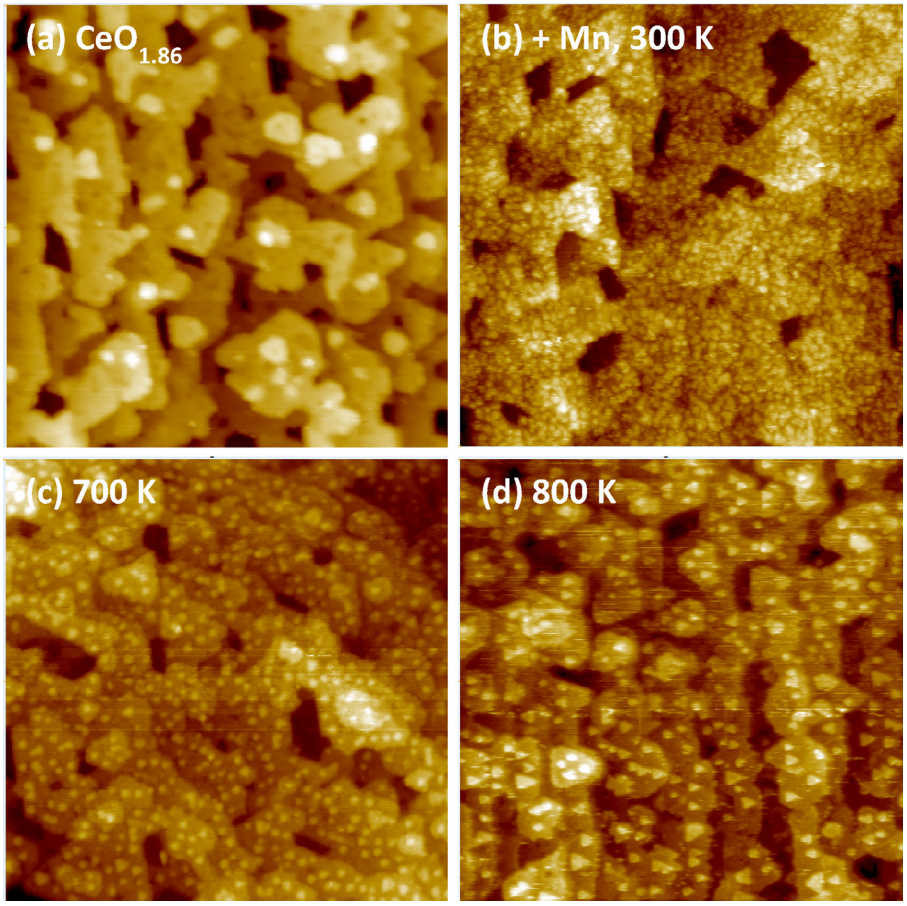

Fig. 3. (a) STM image of a partially reduced $CeO_{1.86}$(111) thin film surface and 0.2 ML Mn deposited on ceria at 300 K (b) as well as after heating to 700 K (c) and 800 K (d). Image sizes are $120 \times 120\,nm^2$.

by the presence of dark features on the terraces. O 1s XPS shoulder peak near the main O lattice peak at 529.3 eV also indicates the film is reduced. Interfacial oxidation and reduction also occur upon Mn deposition on $CeO_{1.86}$ at 300 K. As shown in Fig. 2, Mn 2p spectrum exhibits the same peak profile and doublet binding energy values compared to that from CeO_2. Detailed XPS data analysis suggests Mn is in the formal +2 state on $CeO_{1.86}$ accompanied with ~20% Ce^{4+} reduction to Ce^{3+} as well as the increase in the intensity of the O 1s shoulder peak. Additionally, deposition of 0.2 ML Mn causes ~16% drop of the Ce 3d intensity (data not shown). This is consistent with the formation of small MnO features on the surface. They are on average 0.15 nm high and 2.20 nm wide (Fig. 3b). Heating the surface up to 800 K mainly increases the width of the clusters to 3.10 nm with a slight change of the cluster height to 0.20 nm (Fig. 3c and d). At 800 K, these islands exhibit a well-defined triangular shape which likely expose the (111) plane of MnO [48]. With the same coverage of Mn, more MnO islands were observed on the reduced ceria at 300 K compared to that on CeO_2 which can be attributed to the presence of additional surface defects. After heating to 700 and 800 K, the number of MnO island density are comparable on both reduced and oxidized ceria. As a result of the particle coalescence, the Mn 2p XPS intensity at 800 K reduces to ~66% of its value at room temperature (Fig. 4). In addition, Mn 2p XPS binding energy shifts to a lower energy value which could be related with the particle size effect as demonstrated in our STM results. At 800 K, the peak is centered at ~640.7 eV. This binding energy value is consistent with that of annealed MnO films reported in the literature [48,49].

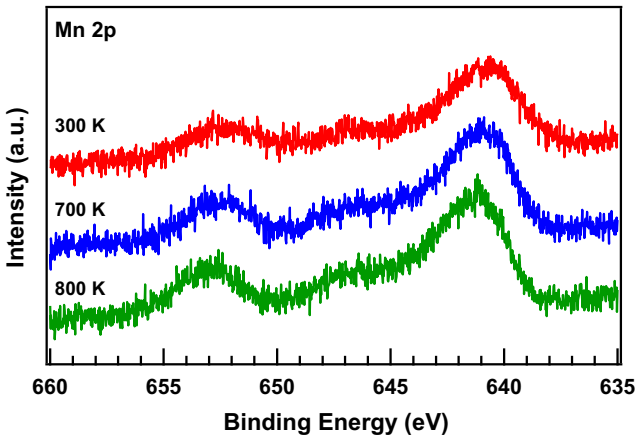

Fig. 4. Mn 2p XPS spectra collected upon Mn deposition on $CeO_{1.86}$ at 300 K as well as after heating to 700 and 800 K.

Our XPS data have suggested that the charge transfer from Mn to ceria occurs upon Mn deposition at 300 K. Mn is oxidized to Mn^{2+} at the cost of Ce^{4+} reduction on both fully oxidized and partially reduced ceria. The interfacial oxidation-reduction process of $Mn + 2CeO_2 \rightarrow Ce_2O_3 + MnO$ is thermodynamically favorable at room temperature based on ΔH_f^{298} of the bulk energetics of oxide formation. Our results are in a great agreement with recent computational study suggesting the formation of Mn^{2+} cations on ceria [30].

Our STM data suggest that the interaction between ceria and Mn occurs at the interface. This is evident with the formation of small two-dimensional Mn-O-Ce complexes. Various adsorption sites are present on ceria for metal ad-atoms. In general, the preferable adsorption sites for less interactive metals are the surface O-O bridge sites on the (111) plane of ceria [33,37,38,50]. For metals that interact strongly with ceria, the O hollow sites are the favorable sites [23,27,30,51]. Computational studies have shown that surface O hollow sites are indeed the preferred adsorption sites for Mn on both fully oxidized and partially reduced ceria [30]. Despite the presence of surface O vacancies on reduced ceria, adsorption of Mn at the missing O lattice is less stable compared to that at O hollow sites. To elucidate the detailed adsorption configuration of Mn on ceria, it is clear that further STM studies with an atomic resolution will be needed. Upon heating, these MnO clusters sinter slightly, primarily aggregating into larger two-dimensional features or arranging to form triangular structures on the ceria surface instead of developing into three-dimensional particles. This is consistent with a strong interaction between Mn and ceria. With heating, diffusion of Mn into ceria cannot be ruled out. It has been shown in the literature that small amounts of Mn cations can be incorporated into ceria to form a solid mixed oxide solution [28–30].

4. Conclusions

In summary, our combined XPS and STM studies demonstrate that Mn dopant can affect both morphology and electronic properties of ceria. Interfacial oxidation/reduction processes occur upon submonlayer coverage of Mn deposition on well-ordered $CeO_x(111)$ thin films at 300 K. Mn is oxidized to Mn^{2+} at the cost of ceria reduction. Atomic-layer high of MnO islands are formed on ceria. Mixed Mn-Ce oxides with controlled structures and compositions can be prepared. It will be of great interest and practical importance to examine the promotional effect of Mn in the chemical behavior of ceria.

Acknowledgement

The authors gratefully acknowledge the financial support from the National Science Foundation (Award Number: CHE1151846).

References

[1] A. Trovarelli, Catalysis by Ceria and Related Materials, Imperial College Press, London, 2002.
[2] G.A. Deluga, J.R. Salge, L.D. Schmidt, X.E. Verykios, Renewable hydrogen from ethanol by autothermal reforming, Science 303 (5660) (2004) 993–997.
[3] J.A. Rodriguez, S. Ma, P. Liu, J. Hrbek, J. Evans, M. Perez, Activity of CeO_x and TiO_x nanoparticles grown on Au(111) in the water-gas shift reaction, Science 318 (5857) (2007) 1757–1760.
[4] Q. Fu, H. Saltsburg, M. Flytzani-Stephanopoulos, Active nonmetallic Au and Pt species on ceria-based water-gas shift catalysts, Science 301 (5635) (2003) 935–938.
[5] P.Y. Sheng, G.A. Bowmaker, H. Idriss, The reactions of ethanol over Au/CeO_2, Appl. Catal. B Environ. 261 (2) (2004) 171–181.
[6] R.J. Gorte, S. Zhao, Studies of the water-gas-shift reaction with ceria-supported precious metals, Catal. Today 104 (1) (2005) 18–24.
[7] J. Stubenrauch, J.M. Vohs, Support effects in the dissociation of CO on $Rh/CeO_2(111)$, Catal. Lett. 47 (1) (1997) 21–25.
[8] X. Wang, R.J. Gorte, J.P. Wagner, Deactivation mechanisms for Pd/ceria during the water-gas-shift reaction, J. Catal. 212 (2) (2002) 225–230.
[9] A. Karpenko, R. Leppelt, J. Cai, V. Plzak, A. Chuvilin, U. Kaiser, R.J. Behm, Deactivation of a Au/CeO_2 catalyst during the low-Temperature water-gas shift reaction and its reactivation: a combined TEM, XRD, XPS DRIFTS, and activity study, J. Catal. 250 (1) (2007) 139–150.
[10] B.M. Reddy, A. Khan, Nanosized CeO_2-SiO_2 CeO_2-TiO_2, and CeO_2-ZrO_2 mixed oxides: influence of supporting oxide on thermal stability and oxygen storage properties of ceria, Catal. Surv. Asia 9 (3) (2005) 155–171.
[11] G. Balducci, P. Fornasiero, R. Dimonte, J. Kaspar, S. Meriani, M. Graziani, An unusual promotion of the redox behavior of CeO_2-ZrO_2 solid-solutions upon sintering at high-temperatures, Catal. Lett. 33 (1–2) (1995) 193–200.
[12] J. Rynkowski, J. Farbotko, R. Touroude, L. Hilaire, Redox behaviour of ceria-titania mixed oxides, Appl. Catal. A Gen. 203 (2) (2000) 335–348.
[13] D.A. Andersson, S.I. Simak, N.V. Skorodumova, I.A. Abrikosov, B. Johansson, Redox properties of CeO_2-MO_2 (M = Ti, Zr Hf, or Th) solid solutions from first principles calculations, Appl. Phys. Lett. 90 (3) (2007) 031909.
[14] G. Dutta, U.V. Waghmare, T. Baidya, M.S. Hegde, K.R. Priolkar, P.R. Sarode, Origin of enhanced reducibility/oxygen storage capacity of $Ce_{1-x}Ti_xO_2$ compared to CeO_2 or TiO_2, Chem. Mater. 18 (14) (2006) 3249–3256.
[15] Z.X. Yang, Y.W. Wei, Z.M. Fu, Z.S. Lu, K. Hermansson, Facilitated vacancy formation at Zr-doped ceria(111) surfaces, Surf. Sci. 602 (6) (2008) 1199–1206.
[16] V. Shapovalov, H. Metiu, Catalysis by doped oxides: CO oxidation by $Au_xCe_{1-x}O_2$, J. Catal. 245 (1) (2007) 205–214.
[17] J.L. Ye, Y.Q. Wang, Y. Liu, H. Wang, Steam reforming of ethanol over $Ni/Ce_xTi_{1-x}O_2$ catalysts, Int. J. Hydrogen Energy 33 (22) (2008) 6602–6611.
[18] G. Avgouropoulos, M. Manzoli, F. Boccuzzi, T. Tabakova, J. Papavasiliou, T. Ioannides, V. Idakiev, Catalytic performance and characterization of Au/doped-ceria catalysts for the preferential CO oxidation reaction, J. Catal. 256 (2) (2008) 237–247.
[19] J.A. Rodriguez, X. Wang, G. Liu, J.C. Hansona, J. Hrbek, C.H.F. Peden, A. Iglesias-Juez, M. Fernandez-Garcia, Physical and chemical properties of $Ce_{1-x}Zr_xO_2$ nanoparticles and $Ce_{1-x}Zr_xO_2(111)$ surfaces: synchrotron-based studies, J. Mol. Catal. A Chem. 228 (1–2) (2005) 11–19.
[20] T. Skala, F. Sutara, M. Cabala, M. Skoda, K.C. Prince, V. Matolin, A photoemission of the interaction of Ga with $CeO_2(111)$ thin films, Appl. Surf. Sci. 254 (2008) 6860–6864.
[21] M. Skoda, M. Cabala, V. Chab, K.C. Prince, L. Sedlacek, T. Skala, F. Sutara, V. Matolin, Sn interaction with the $CeO_2(111)$ system: bimetallic bonding and ceria reduction, Appl. Surf. Sci. 254 (2008) 4375–4379.
[22] T. Staudt, Y. Lykhach, N. Tsud, T. Skala, K.C. Prince, V. Matolin, J. Libuda, Electronic structure of magnesia-ceria catalysts, CO_2 adsorption, and CO_2 activation: a synchrotron radiation photoelectron spectroscopy study, J. Phys. Chem. C 115 (2011) 8716–8724.
[23] Y. Zhou, J. Zhou, $Ti/CeO_x(111)$ interfaces studied by XPS and STM, Surf. Sci. 606 (7–8) (2012) 749–753.
[24] Y. Zhou, J. Zhou, Growth and surface structure of Ti-doped $CeO_x(111)$ thin films, J. Phys. Chem. C 1 (11) (2010) 1714–1720.
[25] T. Skala, N. Tsud, K.C. Prince, V. Matolin, Interaction of tungsten with $CeO_2(111)$ layers as a function of temperature: a photoelectron spectroscopy study, J. Phys. Cond. Matter 23 (2011) 215001.
[26] G. Vari, L. Ovari, C. Papp, H.P. Steinruch, J. Kiss, Z. Konya, The interaction of cobalt with $CeO_2(111)$ prepared on Cu(111), J. Phys. Chem. C 119 (2015) 9324–9333.
[27] M. Baron, H. Abbott, O. Bondarchuk, D. Stacchiola, A. Uhl, S. Shaikhutdinov, H.J. Freund, C. Popa, M.V. Ganduglia-Pirovana, J. Sauer, Resolving the atomic structure of vanadia monolayer catalysts: monomers, trimers, and oligomers on ceria, Angew. Chem. Int. Ed. 48 (2009) 8006–8009.
[28] J. Xu, P. Li, X.F. Song, C.H. He, J.G. Yu, Y.F. Han, Operando raman spectroscopy for determining the active phase in one-dimensional $Mn_{1-x}Ce_xO_{2\pm y}$ nanorod catalysts during methane combustion, J. Phys. Chem. Lett. 1 (10) (2010) 1648–1654.
[29] M.D. Krcha, M.J. Janik, Examination of oxygen vacancy formation in Mn-doped $CeO_2(111)$ using DFT plus U and the hybrid functional HSE06, Langmuir 29 (2013) 10120–10131.
[30] L.C. Hsu, M.K. Tsai, Y.H. Lu, H.T. Chen, Computational investigation of CO adsorption and oxidation on $Mn/CeO_2(111)$ surface, J. Phys. Chem. C 117 (2013) 433–441.
[31] E. Ginting, S.W. Hu, J.E. Thorne, Y. Zhou, J. Zhu, J. Zhou, Interaction of Mn with $CeO_x(111)$ thin films, Appl. Surf. Sci. 283 (2013) 1–5.
[32] D.R. Mullins, P.V. Radulovic, S.H. Overbury, Ordered cerium oxide thin films grown on Ru(0001) and Ni(111), Surf. Sci. 429 (1–3) (1999) 186–198.
[33] J. Zhou, A.P. Baddorf, D.R. Mullins, S.H. Overbury, Growth and characterization of Rh and Pd nanoparticles on oxidized and reduced $CeO_x(111)$ thin films by scanning tunneling microscopy, J. Phys. Chem. C 112 (25) (2008) 9336–9345.
[34] J.L. Lu, H.J. Gao, S. Shaikhutdinov, H.J. Freund, Morphology and defect structure of the $CeO_2(111)$ films grown on Ru(0001) as studied by scanning tunneling microscopy, Surf. Sci. 600 (22) (2006) 5004–5010.
[35] Y. Zhou, J.M. Perket, J. Zhou, Growth of Pt nanoparticles on reducible $CeO_2(111)$ thin films: effect of nanostructures and redox properties of ceria, J. Phys. Chem. C 114 (27) (2010) 11853–11860.
[36] http://www.nist.gov/srd/nist82.cfm.
[37] M. Baron, O. Bondarchuk, D. Stacchiola, S. Shaikhutdinov, H.J. Freund, Interaction of gold with cerium oxide supports: $CeO_2(111)$ thin films vs CeO_x nanoparticles, J. Phys. Chem. C 113 (15) (2009) 6042–6049.
[38] Y. Zhou, E.W. Peterson, J. Zhou, Effect of nature of ceria supports on the growth and sintering behavior of Au nanoparticles, Catal. Today 240 (2014) 201–205.
[39] M.C. Biesinger, B.P. Payne, A.P. Grosvenor, L.W.M. Lau, A.R. Gerson, R.C. Smart, Resolving surface chemical states in XPS analysis of first row transition metals, oxides and hydroxides: Cr, Mn, Fe, Co and Ni, Appl. Surf. Sci. 257 (2011) 2717–2730.
[40] H.W. Nesbitt, D. Banerjee, Interpretation of XPS Mn(2p) spectra of Mn oxyhydroxides and constraints on the mechanism of MnO_2 precipitation, Am. Miner. 83 (1998) 305–315.
[41] L.H. Zhang, Z.Y. Tang, S.L. Wang, D. Ding, M.S. Chen, H.L. Wan, Growth and vibrational properties of MnOx thin films on Rh(111), Surf. Sci. 19–20 (2012) 1507–1511.

[42] P.S. Bagus, E.S. Ilton, Effects of covalency on the p-shell photoemission of transition metals: MnO, Phys. Rev. 73 (2006) 155110.
[43] B.J. Tan, K.J. Klabunde, P.M.A. Sherwood, XPS studies of solvated metal atom dispersed catalysts – evidence for layered cobalt manganese particles on alumina and silica, J. Am. Chem. Soc. 113 (1991) 855–861.
[44] A. Pfau, K.D. Schierbaum, The electronic-structure of stoichiometric and reduced CeO_2 surfaces—an XPS UPS and HREELS study, Surf. Sci. 321 (1–2) (1994) 71–80.
[45] F. Larachi, J. Pierre, A. Adnot, A. Bernis, Ce 3d XPS study of composite $Ce_xMn_{1-x}O_{2-y}$ wet oxidation catalysts, Appl. Surf. Sci. 195 (2002) 236–250.
[46] Y. Wu, Y. Zhang, M. Liu, Z. Ma, Complete catalytic oxidation of o-xylene over Mn-Ce oxides prepared using a redox-precipitation method, Catal. Today 153 (2010) 170–175.
[47] D.R. Mullins, S.H. Overbury, D.R. Huntley, Electron spectroscopy of polycrystalline cerium oxide surfaces, Surf. Sci. 409 (1998) 307–319.
[48] F. Allegretti, C. Franchini, V. Bayer, M. Leitner, G. Parteder, B. Xu, A. Fleming, M.G. Ramsey, R. Podloucky, S. Surnev, F.P. Netzer, Epitaxial stabilization of MnO(111) overlayers on a Pd(100) surface, Phys. Rev. 75 (2007) 224120.
[49] Y. Martynova, M. Soldemo, J. Weissenrieder, S. Sachert, S. Polzin, W. Widdra, S. Shaikhutdinov, H.-J. Freund, CO oxidation over monolayer manganese oxide films on Pt(111), Catal. Lett. 143 (2013) 1108–1115.
[50] J.B. Park, J. Graciani, J. Evans, D. Stacchiola, S.G. Ma, P. Liu, A. Nambu, J.F. Sanz, J. Hrbek, J.A. Rodriguez, Proc. Natl. Acad. Sci. U. S. A. 106 (2009) 4975–4980.
[51] Z.S. Lu, Z.X. Yang, Interfacial properties of NM/CeO_2(111) (NM = noble metal atoms or clusters of Pd, Pt and Rh): a first principles study, J. Phys. Condens. Matter 22 (2010) 475003.